



LAWRENCE
LIVERMORE
NATIONAL
LABORATORY

High aspect ratio hard x-ray (> 100 keV) imager to measure hot electron preheat for indirectly driven capsule implosions on the National Ignition Facility

T. Doppner, E. Dewald, L. Divol, S. Burns, N. Izumi, J. Kline, G. LaCaille, J. McNaney, R. Prasad, C. A. Thomas, S. H. Glenzer, O. Landen, A. Author, S. G. Author, T. Author

May 4, 2012

High-Temperature Plasma Diagnostics Conference
Monterey, CA, United States
May 6, 2012 through May 10, 2012

Disclaimer

This document was prepared as an account of work sponsored by an agency of the United States government. Neither the United States government nor Lawrence Livermore National Security, LLC, nor any of their employees makes any warranty, expressed or implied, or assumes any legal liability or responsibility for the accuracy, completeness, or usefulness of any information, apparatus, product, or process disclosed, or represents that its use would not infringe privately owned rights. Reference herein to any specific commercial product, process, or service by trade name, trademark, manufacturer, or otherwise does not necessarily constitute or imply its endorsement, recommendation, or favoring by the United States government or Lawrence Livermore National Security, LLC. The views and opinions of authors expressed herein do not necessarily state or reflect those of the United States government or Lawrence Livermore National Security, LLC, and shall not be used for advertising or product endorsement purposes.

High aspect ratio hard x-ray (> 100 keV) imager to measure hot electron preheat for indirectly driven capsule implosions on the National Ignition Facility^{a)}

T. Döppner,^{1,b)} E. L. Dewald,¹ L. Divol,¹ C. A. Thomas,¹ S. Burns,¹ P. M. Celliers,¹ N. Izumi,¹ J. Kline,² G. LaCaille,¹ J. M. McNaney,¹ R. Prasad H. F. Robey,¹ S. H. Glenzer,¹ and O. L. Landen¹

¹Lawrence Livermore National Laboratory, P.O. Box 808, Livermore, California 94551, USA

²Los Alamos National Laboratory, Los Alamos, New Mexico 87545, USA

(Presented XXXXX; received XXXXX; accepted XXXXX; published online XXXXX)

(Dates appearing here are provided by the Editorial Office)

We have fielded a multi-pinhole, hard x-ray (> 100 keV) imager to measure the spatially-resolved bremsstrahlung emission from energetic electrons slowing in a plastic ablator shell during indirectly driven implosions at the National Ignition Facility. These electrons are generated in laser plasma interactions, and are a source of preheat to the deuterium-tritium fuel that could limit the compressibility required for ignition and burn. Our hard x-ray imaging measurements allow to set an upper limit to the DT fuel preheat, which we find is acceptable in current capsule implosions on the NIF.

I. INTRODUCTION

Achieving high neutron-yield inertial confinement fusion implosions requires high and efficient compression of the deuterium-tritium (DT) fuel. For a given driver, keeping the DT fuel entropy low (i.e. solid DT near Fermi degeneracy) is crucial for obtaining high areal densities.¹ Current experiments² of the National Ignition Campaign (NIC)³ aim at obtaining such low entropy implosion under indirect-drive conditions by controlling the precise merging of 4 shock waves at the inside of the DT ice layer of an ignition capsule. One possible obstacle to high compression is preheat of the DT by energetic electrons⁴ produced during laser-plasma interaction (LPI) inside the hohlraum.⁵ The resulting increase in adiabat, defined as the ratio of total deuterium-tritium fuel pressure to Fermi pressure, has to remain small relative to the adiabat $\alpha = 1.5$ of the dense DT fuel after shock compression to achieve ignition on the National Ignition Facility (NIF).

The spatially integrated hot electron generation in NIC implosion experiments is routinely recorded by the FFLEX diagnostics.⁶ These measurements allow for an inference of preheat based on certain assumptions, in particular homogeneous hot electron sourcing and transport. In order to test this hypothesis we have built and fielded a hard x-ray imager to measure the spatially resolved bremsstrahlung emission above 100 keV from fast electrons slowing down in the plastic (CH) ablator. A simple formula, balancing bremsstrahlung emission and stopping power for energetic electrons, is used to relate the bremsstrahlung emission I_{Br} to the amount of energetic electrons:⁷

$$I_{Br} \left(\frac{\text{keV}}{\text{keVsr}} \right) = \frac{6.3}{4\pi} \times 10^9 Z^* E_{hot}(\text{J}) e^{1-h\nu/kT_{hot}}, \quad (1)$$

with $Z^* = \langle Z^2 \rangle / \langle Z \rangle$ the average atomic number, E_{hot} the energy in energetic electrons, and T_{hot} the characteristic temperature of the hot electron distribution. I_{Br} scales linearly

with Z since the bremsstrahlung efficiency scales as Z^2 while the electron stopping power scales as Z . Note that, according to Eq. (1), ~ 15 times more electrons are necessary to yield the same bremsstrahlung emission from stopping in CH ($Z^* = 5.3$) compared to stopping in Au ($Z = 79$). Recently we reported on the first preheat measurement in a symcap experiment (shot N110214), in which the DT fuel layer is replaced by an equivalent mass of CH. We derived an upper bound of adiabat increase of 3.5% which is acceptable within the current error budget roll-up.⁸ Here we report on details of the polar hard x-ray imager used for this measurement.

II. POLAR HARD X-RAY IMAGER (PHXI)

For the description of the general experimental configuration we refer the reader to Refs. 2 and 8. The polar hard x-ray imager filtering configuration used on shot N110214 is shown in Fig. 1. We are utilizing a regular 1x imaging snout for which the front surface of the pinhole package is located 640 mm from the center of the target, towards the top of the target chamber. This allows an unobstructed view through the 3.1 mm diameter laser entrance hole (LEH) towards the capsule.

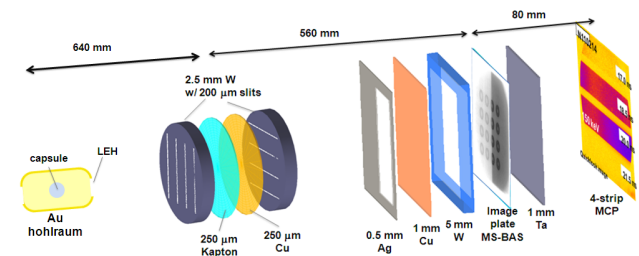


FIG. 1. (Color online). Filter configuration for the polar hard x-ray imager with high aspect ratio pinholes provided by crossing 200 μm wide slits in 2.5 mm tungsten plates (not drawn to scale). Primary imaging data are time integrated, and recorded with an image plate located in the main filter pack.

^{a)}Contributed (or Invited) paper published as part of the Proceedings of the 19th Topical Conference on High-Temperature Plasma Diagnostics, Monterey, California, May, 2012.

^{b)}Author to whom correspondence should be addressed: doepner1@llnl.gov.

In order to suppress the direct hard x-ray background to an acceptable level, a Ta or W pinhole substrate of at least 5 mm thickness is required. High aperture pinholes are challenging to fabricate into these high-Z materials. We used wire electrical discharge machining (wire EDM) to cut 200 μm wide slits into 2.5 mm thick tungsten plates. By crossing 2 plates with 4 slits each we created an array of 16 pinholes. The 200 μm pinhole size turned out to be good compromise between 425 μm spatial resolution and obtaining an acceptable signal level in the highest energy channel of the instrument. Sandwiched between the pinhole plates is a 250 μm Kapton layer to absorb the soft x-ray load, and a 250 μm copper filter. This combination of filter materials was designed to prevent debris from penetrating further down the imaging snout.

For the main filter pack in the kinematic base mount at 560 mm from the pinholes, Fig. 1 shows the configuration used on shot N110214. Here we recorded a total of 16 images in 2 energy channels. The lower energy channel had 1 mm of Cu in addition to the filtering in the nose cone described above. The higher energy channel had an additional 0.5 mm of Ag. Fig. 2 shows calculated signal levels for these two channels (84 keV and 125 keV) along with the response of a softer channel at 65 keV channel (1 mm Al filter instead of 1 mm Cu) that was used on shot N101111. The numbers quoted are mean energies calculated from the displayed profiles. The images corresponding to these 3 response curves are shown in Fig. 4.

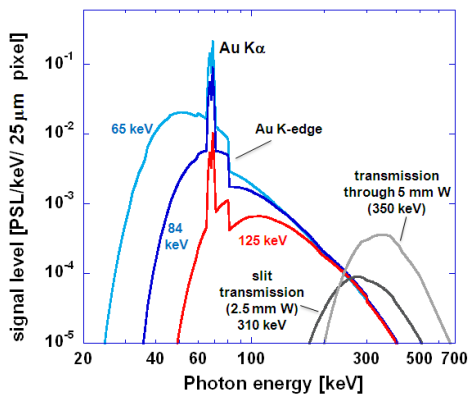


FIG. 2: (color online). Sensitivity curves for 3 spectral channels and background contributions that include the measured bremsstrahlung spectrum, filter transmissions, IP sensitivity, and transmission through the 80 μm thick hohlraum Au endcap, in comparison with the background transmitted through the pinhole substrate.

In order to calculate the response curves shown in Fig. 2, in addition to the filter transmissions, and taking into account the different view factors for images and background signals, we used the spatially integrated hard x-ray emission spectrum as measured by FFLEX,^{6,8} the image plate sensitivity, and the transmission through the 80 μm thick Au hohlraum endcap, cf. Fig. 3. The 2-temperature hard x-ray spectrum is typical for gas-filled hohlraum experiments on the NIF, with the lower temperature component corresponding to energetic electrons generated by stimulated Raman scattering⁹ (SRS) ($T_1=18$ keV, $E_1=50 \pm 20$ kJ), and a hot component likely due to interaction around quarter-critical density ($T_2=110$ keV, $E_2=1.0 \pm 0.3$ kJ). The best fit to the 10 FFLEX channels includes Au K- α line emission at 67 and 69 keV which is 8.5 times higher than the continuum which appears as a prominent feature in the energy content of the images. If the source spectrum was flat, the mean energies would be 58, 80, and 115 keV for the imaging channels.

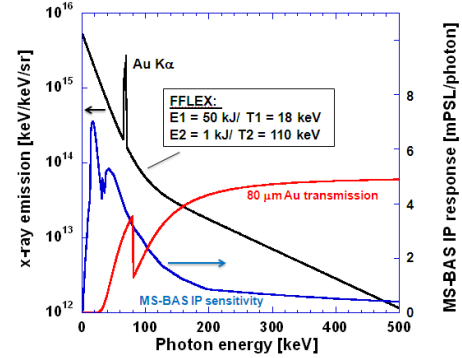


FIG. 3: (color online). Hard x-ray emission spectrum as measured by FFLEX, MS-BAS image plate response and transmission through the 80 μm thick Au hohlraum endcap.

We use imaging plate detectors (BAS-MS) with absolutely calibrated x-ray response and fading characteristics¹⁰ to record time-integrated images. For the x-ray response above 100 keV we extrapolated to data and simulations that were collected at ~ 660 keV.¹¹ It takes between 6 and 24 hours to retrieve the IPs from the NIF target chamber. Hence the signal fading for these MS plates is typically between 65 and 80 %. The IP is located at 560 mm behind the pinholes, resulting in a magnification of $M = 0.89$. Along with the 200 μm pinhole size this results in a spatial resolution of 425 μm . Due to the relatively large pinhole stand-off the snout alignment is done using the wide field-of-view Chamber Interior Viewing System (CIVS) which introduces a potential alignment error of ± 3 mm. The magnification and thus the insertion depth can be accurately determined from the separation of the images since the pinhole array has been characterized with x-ray shadowgraphs.

III. DATA

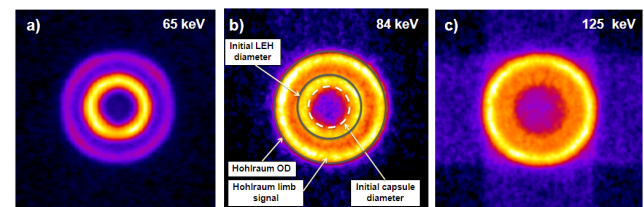


FIG. 4: (color online) polar hard x-ray images between 60 keV and 125 keV. Mean photon energies are given, the corresponding PHXI response curves are given in Fig. 2.

Fig. 4 shows images taken in 3 different energy channels. While the 65 keV image was taken on shot N101111, the two high energy images were recorded on N110214. Both shots were symcap experiments using the same hohlraum and capsule geometry, and a similar laser drive and resulting hot electron generation. The main features are labeled in Fig. 4b, and the initial diameters of the hohlraum (5.44 mm), the LEH (3.1 mm), and the capsule (2.2 mm) are indicated. One prominent feature is the emission from just inside the LEH radius which is dominating the low energy channel, and is absent in the highest energy channel. Equatorial hard x-ray imaging¹² confirms that this feature is due to interaction of the incoming laser beams with ablated material just inside and outside of the LEH. From the spectral intensity dependence in equatorial images up to 55 keV we find that the emission from outside the LEH is dominated by a temperature component of 2 ± 1 keV. In order to avoid that this LEH emission is corrupting the signal from the capsule at the

center of the hohlraum, for the preheat analysis we focus on the highest energy channel image. While for the lower energy channels individual images are displayed, Fig. 4c is an average over 8 images. One of the striking features is the cross-like background that is due to the transmission through the slits. As shown in Fig. 2, the mean energy of this contribution is 310 keV. We find that the measured signal level of this 1D image is very close to prediction which provides an important confirmation for the FFLEX measurement and the sensitivity curves used here. The background-subtracted image that is used for further analysis is shown in Fig. 2 of Ref. 8.

IV. DISCUSSION OF BACKGROUND SIGNALS

In order to achieve acceptable signal/ noise ratios as demonstrated in Ref. 8 the background signals need to be minimized. In this section we will discuss background mitigation strategies, and the impact of Compton scattering on the point spread function.

A. Background signal mitigation

Besides direct transmission through the 5 mm tungsten substrate there is potentially fluorescence from components in the nose-cone, and Compton scattering from various components in the target chamber. Since for x-rays above 50 keV a substantial fraction passes the imaging plate, even fluorescence or backscatter from the back of the diagnostic can cause an additional background signal. We have tested the latter by placing a half aperture, 0.5 mm thick Ta filter (>10% transmission at $E > 120$ keV) at the *back* of the image plate. We found that the background signal was reduced by a factor of 3 in the area that was covered with Ta compared to the area that was left open. On subsequent shots we started using full aperture, 1 mm thick Ta filters to protect the back of the image plate, cf. Fig. 1. We have checked that Compton backscatter does not introduce an additional background component since most of it is re-absorbed within the Ta filter.

The main background contribution that remains is due to fluorescence or backscatter from the front of the imaging snout. We have increased the shielding of the nose cone by replacing aluminum with stainless steel which did not yield a significant improvement. The best mitigation strategy of this background component seems to be adding all of the spectral filtering close to the image plate. However, this has a potential impact on the point spread function as discussed in the following section.

B. Compton Scattering from Filters

At energies above 100 keV in copper the Compton scattering cross section becomes comparable, and at $E_{ph} > 150$ keV it starts to exceed the photo ionization cross section. The Compton scattering cross section is rather independent on photon energy for the energy range relevant for this investigation. For copper, at 100 keV a 1 mm thick Cu filter will Compton scatter ~10% of the incoming radiation. According to the Klein-Nishina formula, the forward scattering is enhanced when going to higher photon energies. For example, at 120 keV forward scattering is a factor of 2 higher than backscatter.

Compton scattering from objects close to the detector can add a low signal level, large radius foot to the real signal, thus altering the point spread function. This becomes an issue if one aims at observing features with low signal levels close to strong features. This is the case for the application under consideration here where the hohlraum signal (and the LEH emission in the lower energy channels) is up to 10x of the expected capsule

signal in the center of the image. The particular issue here is that the forward scattered component would add up more strongly in the center of the image compared to regions outside the hohlraum which would make the background subtraction difficult. We have carefully simulated this effect, and find that it could add 2% of the maximum hohlraum signal to the center of the image, which could be accounted for emission from the capsule. This has to be compared to the expected signal from the capsule which is on order of 10% of the maximum hohlraum signal. By separating the filters by 5 mm from the IP this effect can be reduced by a factor of four to 0.5%. To accomplish this, in the current design we use a 5 mm thick tungsten frame that additionally casts a shadow on the IP and helps to measure the hard x-ray background transmitted through the pinhole substrates. Further separation is impossible within the current snout design.

V. SUMMARY

We have built and successfully fielded a high-aperture hard x-ray (> 100 keV) imager to measure bremsstrahlung emission from a compressing CH capsule in an ignition-scale hohlraum on the NIF. While we discussed the details and design consideration of this imager here, Ref. 8 reported on the first hot-electron preheat measurement in a NIC hohlraum. We found an upper limit of 570 ± 250 J of energetic electrons absorbed in the capsule ablator towards the end of the laser pulse, which translates to an acceptable 3.5% increase in adiabat for current NIC cryogenic DT implosions.⁸

VI. Acknowledgements

We thank the NIF operations, laser performance, target diagnostics, data analysis, data visualization, and target fabrication teams. This work was performed under the auspices of the U.S. Department of Energy by Lawrence Livermore National Laboratory under Contract No. DE-AC52-07NA27344 and by Los Alamos National Laboratory under Contract No. DE-AC52-06NA25396.

¹J. Lindl, et al., Phys. Plasmas **11**, 339 (2004).

²S. H. Glenzer et al, Phys. Rev. Lett. **106**, 085004 (2011).

³E. Moses, et al., Phys. Plasmas **16**, 041006 (2009).

⁴V.A. Smalyuk et al., Phys. Rev. Lett. **100**, 185005 (2008).

⁵S.P. Regan et al., Phys. Plasmas **17**, 020703 (2010).

⁶E.L. Dewald, et al., Rev. Sci. Instrum. **81**, 10D938 (2010).

⁷R.P. Drake, R.E. Turner, B.F. Lasinski, E.A. Williams, K. Eastbrook, W.L. Kruer, E.M. Campbell, and T. W. Johnston, Phys. Rev. A **40**, 3219 (1989).

⁸T. Döppner et al., Phys. Rev. Lett. **108**, 135006 (2012).

⁹A.A. Offenberger, R. Fedosejevs, W. Tighe, and W. Rozmus, Phys. Rev. Lett. **49**, 371 (1982).

¹⁰B.R. Maddox et al., Rev. Sci. Instrum. **82**, 023111 (2011).

¹¹C.D. Chen, N. Izumi, private communication.

¹²H.S. Park et al., Rev. Sci. Instrum. **81**, 10D938 (2010).